archives
of thermodynamics
Vol. **40**(2019), No. 4, 3–20
DOI: 10.24425/ather.2019.130005

Unconfined laminar nanofluid flow and heat transfer around a rotating circular cylinder dissipating uniform heat flux in the steady regime

RAFIK BOUAKKAZ[a*]
ABDED EL OUAHED OUALI[b]
YACINE KHELILI[c]
SALHI FAOUZI[d]
ILYES TIAUIRI[A]

[a] Military Academy of Cherchell, Tipaza, Algeria

[b] Faculté des Sciences et de la Technologie, Université de Biskra

[c] Department of Mechanical Engineering, University Saad Dahlab, Blida, Algeria

[d] Département de Génie Mécanique, Université Mouloud Mammeri Tizi ouzou, Algérie

Abstract In this work, steady flow-field and heat transfer through a copper-water nanofluid around a rotating circular cylinder, dissipating uniform heat flux, with a constant non-dimensional rotation rate varying from 0 to 5 was investigated numerically using a finite-volume method for Reynolds numbers from the range 10–40. Furthermore, the range of nanoparticle volume fractions considered is 0–5%. The variation of the local and the average Nusselt numbers with Reynolds number, volume fractions, and rotation rate are presented for the range of conditions. The average Nusselt number is found to increase with increasing the nanoparticle volume fractions and decrease with increasing value of the rotation rate.

Keywords: Copper nanoparticles; Rotating circular cylinder; Dissipating uniform heat flux; Steady regime

*Corresponding Author. Email: r.bouakkaz@gmail.com

Nomenclature

C_D	–	drag coefficient
C_L	–	lift coefficient
C_p	–	specific heat capacity, J/(kgK)
D	–	drag force, N
D_t	–	diameter of the cylinder, m
L	–	lift force, N
k	–	thermal conductivity, W/(m K)
Nu	–	average Nusselt number
Nu_0	–	average Nusselt number for the stationary cylinder
Nu	–	local Nusselt number
$\overline{\mathrm{Nu}}$	–	average Nusselt number
$\overline{\mathrm{Nu}_0}$	–	average Nusselt number for the stationary cylinder
p	–	local pressure, $\mathrm{N/m^2}$
q	–	heat flux, $\mathrm{W/m^2}$
q_w	–	uniform heat flux, $\mathrm{W/m^2}$
Re	–	Reynolds number
Pr	–	Prandtl number
T_∞	–	free-surface temperature, K
U_∞	–	free-stream velocity, m/s
u	–	stream-wise velocity, m/s
v	–	cross-stream velocity, m/s
x, y	–	Cartesian coordinates

Greek symbols

α	–	non-dimensional rotation rate
φ	–	nanoparticle volume fractions
ϕ	–	angular displacement from the front stagnation point
θ	–	non-dimensional temperature
μ	–	dynamic viscosity, Pa s
ν	–	kinematic viscosity, $\mathrm{m^2/s}$
ρ	–	density, $\mathrm{kg/m^3}$
ω	–	vorticity on the surface of the cylinder, 1/s
Ω	–	constant angular velocity of the cylinder rotation, rad/s

Subscripts

f	–	base fluid
nf	–	nanofluid
s	–	solid nanoparticles

1 Introduction

In recent years, fluid flow and heat transfer around rotating cylinders has been a subject of great interest for researchers due to its high applicability in many industrial developments. In such problems, the fluid flow

and heat transfer depend on the Reynolds number (Re) and rotation rate (α), defined as the ratio of rotational velocity of the cylinder wall to the incoming free stream flow velocity. The authors of the paper [1] using standard boundary conditions namely constant wall temperature (CWT) studied numerically the effect of rotation rate on the flow and heat transfer across a rotating cylinder in the range $0 \leq \alpha \leq 6$ with Re number varying from 20–160. They concluded that the rotation can be used as a drag reduction and heat transfer suppression technique. The suppression of von Karman street was also reported numerically in [2] for Reynolds numbers of 20–200 and rotation rate of 0–6 at Prandtl number (Pr) of 0.7. For steady regime, a well-organized numerical study was published in [3]. In that paper, the numerical calculations were solved via the finite volume method in order to examine the characteristics of flow and heat transfer for varying rotation rate (α = 0–5) in the Reynolds number range 1–35 and Prandtl numbers range 0.7–100. They found that the average Nusselt number increases with increasing Prandtl number for the fixed value of the Reynolds number for the particular value of rotation rate. Also, free stream flow and forced convection heat transfer across a rotating circular cylinder for Prandtl number between 0.7 and 67 at Reynolds number in the range of 5 to 40 was carried by [4]. In depth analysis, they revealed that the heat transfer across the cylinder becomes increasingly independent of the thermal boundary condition, i.e., UHF or CWT. Moreover, the authors [5] using uniform dissipating heat flux boundary conditions (UHF) investigated numerically the free stream flow and forced convection heat transfer across a rotating cylinder for Reynolds numbers of 20–160 and a Prandtl number of 0.7. Their results show that, at higher rotational velocity, the Nusselt number is almost independent of Reynolds number and the thermal boundary conditions. In past studies, the fluids used have a low value of thermal conductivity, which limits the heat transfer. For this reason, there are several methods to improve the heat transfer characteristics, which consist in adding high conducting solid particles in the base fluid. The resulting fluid is called 'nanofluid'[6–8]. The steady flowfield and heat transfer through a copper-water nanofluid around circular cylinder was numerically simulated by [9]. The values of vorticity, pressure coefficient, recirculation length are increased by the addition of nanoparticles into the base fluid. Subsequently, [10] examined the effect of heat treatment process with a new cooling medium (nanofluid), which contains water with Cu, Ag or Al_2O_3 particles, on heat transfer characteristics and

mechanical properties of an unsteady continuous moving cylinder in the thermal forces. They reported that the Al_2O_3 nanofluid is the best type of nanofluid for improving the mechanical properties of the surface (increase the heat flux). This nanofluid is also the best type for decreasing the surface shear stress. Recently, [11] have focused on numerical study of heat transfer phenomena over an isothermal cylinder, for low Reynolds number flow of nanofluid. Heat transfer characteristic and flow over the stationary cylinder has been studied for water based copper nanofluid with different solid fraction values. They have shown that presence of nanoparticle has no effect on point of flow separation for a fixed Reynolds number because the effect of buoyancy force has not been taken into consideration. On the other hand, [12] have studied the momentum and forced convection heat transfer for a laminar and steady free stream flow of nanofluids past a square cylinder. Different nanofluids consisting of Al_2O_3 and CuO with base fluids such as water and a 60/40 (by mass) ethylene glycol and water mixture were selected to evaluate their superiority over conventional fluids. They showed that for any given particle diameter there is an optimum value of particle concentration that results in the highest heat transfer coefficient. The fluid flow and heat transfer around a square cylinder utilizing Al_2O_3-H_2O nanofluid over low Reynolds numbers varied within the range from 1 to 40 and the volume fraction of nanoparticles (φ) varied within the range of $0 < \varphi < 0.05$ was investigated by [13]. They found that increasing the nanoparticles volume fractions augments the drag coefficient. Moreover, pressure coefficient increases by increasing the solid volume fraction for sides where pressure gradient is inverse but for sides where the pressure gradient is favourable the pressure coefficient decreases. The present investigation had been motivated by increased interest and research in potential improvements in heat transfer characteristics using nanofluids. Effort has been made to investigate numerically the steady flow of nanofluid and heat transfer, dissipating uniform heat flux, characteristics of a rotating circular cylinder for a range of Reynolds numbers ($10 \leq \mathrm{Re} \leq 40$) and particle volumetric concentrations ranging from 0% to 5% for rotation parameters ($0 \leq \alpha \leq 5$) in the two-dimensional laminar flow regime.

2 Problem statement, governing equations, and boundary conditions

The system here consists of a 2D infinitely long circular cylinder having a diameter D_t which is rotating in a counter-clockwise direction with a constant angular velocity of Ω and dissipating uniform heat flux $q = q_w$. It is exposed to a constant free stream velocity of U_∞ at a uniform temperature of T_∞ at the inlet. The nanoparticles are assumed to be uniform shape and size. In addition, we have assumed that nanoparticles are in thermal equilibrium state and flowing at the same velocity. Flow configuration is shown in Fig. 1. It is interesting to remind that the Reynolds and rotation rate can be expressed as $\mathrm{Re} = U_\infty D_t/\nu$ and $\alpha = \Omega D_t/2U_\infty$, where ν is the kinematic viscosity of water.

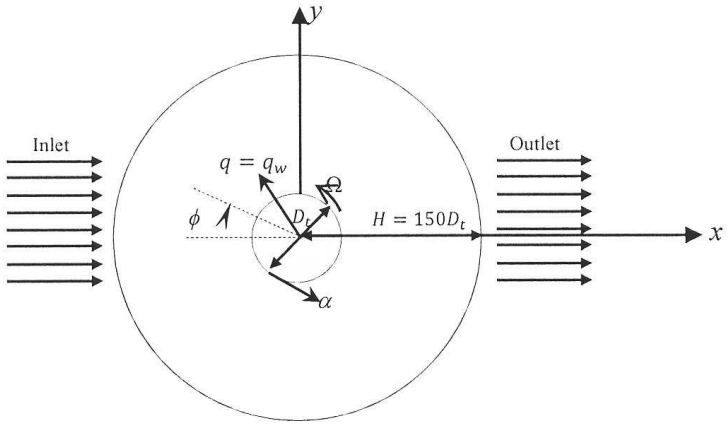

Figure 1: Schematic of the unconfined flow past a rotating cylinder dissipating uniform heat flux.

2.1 Governing equations and boundary conditions

The governing partial differential equations here are the Navier-Stokes and energy equations in two dimensions and steady state nanofluid flow around a rotating circular cylinder are:
continuity equation

$$\frac{\partial U}{\partial X} + \frac{\partial V}{\partial Y} = 0\,, \tag{1}$$

momentum equations

$$U\frac{\partial U}{\partial X}+V\frac{\partial U}{\partial Y}=-\frac{\partial P}{\partial X}+\frac{1}{Re}\frac{v_{nf}}{v_f}\left(\frac{\partial^2 U}{\partial X^2}+\frac{\partial^2 U}{\partial Y^2}\right), \tag{2}$$

$$U\frac{\partial V}{\partial X}+V\frac{\partial V}{\partial Y}=-\frac{\partial P}{\partial Y}+\frac{1}{Re}\frac{v_{nf}}{v_f}\left(\frac{\partial^2 V}{\partial X^2}+\frac{\partial^2 V}{\partial Y^2}\right), \tag{3}$$

energy equation

$$U\frac{\partial \theta}{\partial X}+V\frac{\partial \theta}{\partial Y}=\frac{1}{\mathrm{RePr}}\frac{\alpha_{nf}}{\alpha_f}\left(\frac{\partial^2 \theta}{\partial X^2}+\frac{\partial^2 \theta}{\partial Y^2}\right), \tag{4}$$

where

$$U=\frac{u}{U_\infty}, \quad V=\frac{v}{U_\infty}, \quad X=\frac{x}{D_t}, \quad Y=\frac{y}{D_t}, \quad P=\frac{p}{\rho_{nf}U_\infty^2},$$

$$\theta=\frac{T-T_\infty}{(q_w D_t/k_f)}, \quad \mathrm{Pr}=\frac{\nu_f}{\alpha_f}, \quad \mathrm{Re}=\frac{U_\infty D_t}{\nu_f}.$$

Here the capital letters represent dimensionless combinations of physical quantities, respectively, U and V are the non-dimensional velocity components along X and Y axes, θ is the non-dimensional temperature, P is the non-dimensional pressure, whereas small letters u, v, p, represent physical quantities velocity components and pressure, respectively, T is the temperature, ρ is density, a the thermal diffusivity, and ν the kinematic viscosity. The subscript nf stands for nanofluid, the subscripts f and s stand for base fluid and solid nanoparticles, respectively. The thermophysical properties taken from [9], for the base fluid and copper oxide (at 300 K) are shown in Tab. 1.

Table 1: Thermophysical properties of the base fluid and the Cu nanoparticles.

Property	Units	Water	Copper
Heat capacity, C_p	J/kgK	4179	385
Density, ρ	kg/m^3	997.1	8.933
Thermal conductivity, k	W/m K	0.613	401

The effective density, thermal diffusivity, heat capacitance, effective dynamic viscosity and effective thermal conductivity of the nanofluid are calculated using the following expressions:

$$\rho_{nf} = (1-\varphi)\,\rho_f + \varphi\rho_s\,, \tag{5}$$

$$(\rho C_p)_{nf} = (1-\varphi)\,(\rho C_p)_f + \varphi\,(\rho C_p)_s\,, \tag{6}$$

$$\alpha_{nf} = k_{nf}/\,(\rho C_p)_{nf}\,, \tag{7}$$

$$\mu_{nf} = \frac{\mu_f}{(1-\varphi)^{2.5}}\,, \tag{8}$$

$$k_{nf} = k_{bf}\left[\frac{(k_s+2k_f)-2\varphi\,(k_f-k_s)}{(k_s+2k_f)+\varphi\,(k_f-k_s)}\right]\,, \tag{9}$$

where φ is the solid volume fraction.

2.2 Boundary conditions

The dimensionless boundary conditions for the flow across a circular cylinder can be written as (Fig.1). The left-hand arc is the inflow section or upstream section, where there is the Dirichlet-type boundary condition for the Cartesian velocity components

$$U = 0\,, \quad V = 0\,, \quad \text{and} \quad \theta = 0\,. \tag{10}$$

The right-hand arc represents the outflow boundary, where it is considered that the diffusion flux in the direction normal to the exit surface is zero for all variables

$$\frac{\partial U}{\partial X} = \frac{\partial V}{\partial X} = \frac{\partial \theta}{\partial X} = 0\,. \tag{11}$$

Finally, the dimensionless peripheral or tangential velocity is prescribed on the surface of the cylinder, along with a no-slip boundary condition

$$U = -\alpha\sin\phi\,, \quad V = -\alpha\cos\phi\,, \quad \frac{\partial\theta}{\partial n_s} = -1\,, \tag{12}$$

where n_s is the normal unit direction vector away from the cylinder surface and ϕ the angular displacement from the front stagnation point.

The Nusselt number (Nu) is defined as the ratio of convective to conductive heat transfer across (normal to) the boundary.

2.3 Force coefficients

Two relevant parameters computed from the velocity and pressure fields are the drag and lift coefficients, which represent dimensionless expressions of the forces that the fluid produces on the circular cylinder. These are defined, respectively, as follows:

$$C_L = \frac{L}{D_t \rho U_\infty^2}\,, \quad C_D = \frac{D}{D_t \rho U_\infty^2}\,, \tag{13}$$

where D is the drag force and L is the lift force with respect to the centre of the cylinder.

3 Numerical details

The steady, laminar, segregated solver was employed here to solve the incompressible flow on the collocated grid arrangement. Semi implicit method for the pressure linked equations (SIMPLE) was used to solve Navier-Stokes and energy equations for above outlined boundary conditions. Second order upwind scheme is used to discretize the convective terms of momentum equations, whereas the diffusive terms are discretized by central difference method. A convergence criterion of 10^{-8} is used for continuity, and x-y components of momentum equations, while for energy equation the criteria of convergence was 10^{-10}.

3.1 Domain independence study

The mesh used for all the two-dimensional computations consisted of 40 000 quadrilateral cells and 40 200 nodes. The cylinder (of diameter D_t) resides in a computational domain whose outer edges located at a distance of H from the centre of the cylinder (Fig. 1). There are N_t points in the circumferential direction on the cylinder surface and the radial thickness of the first layer of cells, (i.e. cells attached to the wall) is h_{Dt}. The location of the outer boundary of the domain is expected to become more crucial for larger values of α [2,3]. In this study, following authors [3,4], the computational domain extends 150 times the diameter of the cylinder in all directions. The grids sensitivity analysis is performed for Re = 40 and $\varphi = 0.05$. Table 2 lists the details for the meshes that were employed. As a Regarding the influence of the number of grid points on the average Nusselt number on the wall of cylinder, it was decided to carry out the computations in this work with mesh M2.

Table 2: Effect of grid number on averaged Nusselt number at Re = 40, Pr = 4.76 ($\varphi = 0.05$) for $\alpha = 0$ and $\alpha = 5$.

Mesh	No. of cells	N_t	h_{Dt}/D_t	$\overline{\mathrm{Nu}}$	
				$\alpha = 0$	$\alpha = 5$
M1	32000	160	0.0015	9.3447	5.5840
M2	40000	200	0.0010	9.3766	5.6132
M4	50000	250	0.0010	9.3688	5.6169

Table 3: Comparison of Nu number computed in the present study with literature data (Pr = 0.7).

Re = 20			
α	Data from [5]	Present study	Relative error (%)
0	2.7499	2.7382	0.43
1	2.5312	2.5632	1.26
2	2.2811	2.3067	1.12
3	2.2187	2.2490	1.37
4	2.2512	2.2671	0.71
5	2.3124	2.2878	1.06
Re = 40			
α	Data from [5]	Present study	Relative error (%)
0	3.7499	3.7618	0.32
1	3.4062	3.4293	0.68
2	3.0123	3.0200	0.25
3	2.9374	2.9548	0.59
4	3.0312	3.0174	0.45
5	3.0312	3.0473	1.53

4 Results and discussion

4.1 Comparison with other results

The first step was to validate the problem set-up, the choice of numerical methods and mesh attributes by comparing results from our numerical simulations with the results obtained from literature. The outcomes in-

cluded in the comparison were the mean Nusselt number, as well as lift and drag coefficients. Besides, Tab. 4 compares the lift and drag coefficients computed here with existing results. We have noted that the lift coefficient values are in excellent agreement with the numerical data reported by other researchers, but discrepancies in the values of the drag coefficient are larger; the drag coefficients are so small that the relative errors are magnified.

Table 4: Comparison between the lift and drag coefficients computed in the present study with values given by literature data.

Re	α	C_D			C_L		
		Present study	Paper [5]	Relative error (%)	Present study	Paper [5]	Relative error (%)
40	0	1.5030	1.504	0.066	0.0	0.0	0.00
40	1	1.3132	1.315	0.150	-2.5817	-2.6013	0.75
40	4	-0.0380	-0.052	26.920	-16.0830	-16.0330	0.31

4.2 Streamlines patterns

The streamlines around cylinder are compared between base fluid and nanofluid ($\varphi = 0.05$) in Fig. 2 at Reynolds number of 20 and 40 for α of 0 and 5. At fixed cylinder and for high Reynolds number the recirculation bubble becomes big and strong at the downstream side of the cylinder for both the base fluid and nanofluid. However, in nanofluid the center of bubbles is slightly pushed away from the surface of the cylinder comparing the with base fluid. On increasing the value of the rotation rate, the stagnation point lies above the cylinder, in the region where the direction of the free stream opposes the motion induced by the rotating cylinder. Furthermore, for the highest Reynolds number, the stagnation point moves upwards (dashed line indicates the y coordinates position of stagnation point).

4.3 Isotherm patterns

The isotherms profiles around the rotating cylinder for Reynolds number of 40 for α of 0 and 5 are compared between base fluid and nanofluid ($\varphi = 0.05$) in Fig. 3. Clearly, the temperature distribution contours for

the base fluid are overlaid with that for nanofluid. This can be explained as the addition of solid particles to the base fluid increases the Reynolds number of nanofluid. Hence, a higher capacity of transferring the heat from the cylinder. For a stationary cylinder ($\alpha = 0$), it is obvious from Fig. 3 that the isotherms have maximum density close to the front surface of the cylinder; this indicates high values of the local Nusselt number near the front stagnation point on the front surface as compared to other points on the cylinder surface. On increasing the value of the rotation rate, the maximum density of the isotherm shifts from the front surface towards the bottom surface of the rotating cylinder (rotating counter-clockwise).

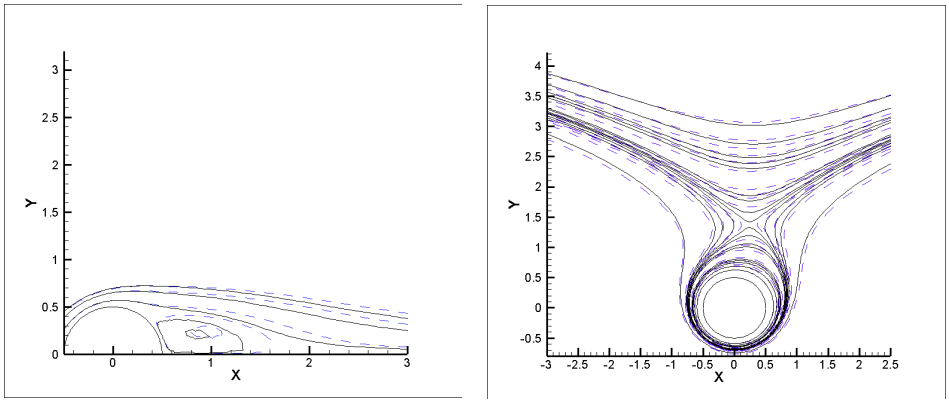

Figure 2: Streamline contours for the flow around the cylinder (solid line refers to the base fluid and dashed line refers to the nanofluid with the volume of solid.

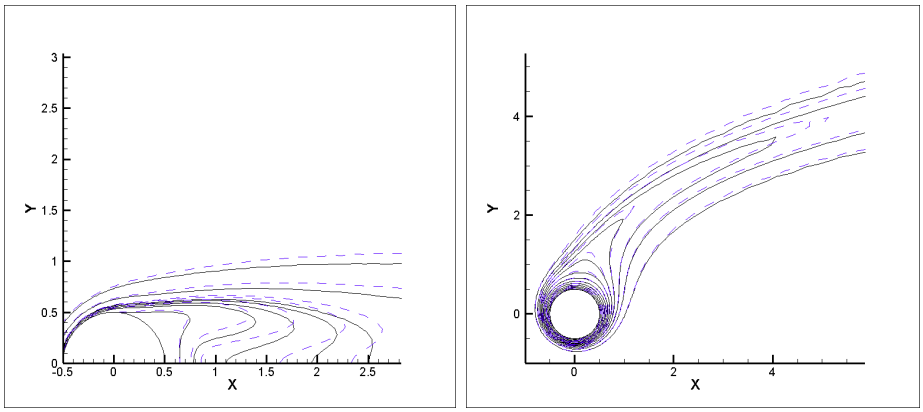

Re = 40

Figure 3: Temperature contours for the flow around the cylinder (solid line refers to the base fluid and dashed line refers to the nanofluid with solid volume fraction 0.05) at Re = 40.

4.4 Local Nusselt number

Figure 4 shows the variation of local Nusselt number on the surface of the cylinder with increase in Reynolds number for various rotation rates α and volume fraction. When the solid concentration increases the thermal conductivity improves and consequently the local Nusselt number. Additionally, the thermal boundary layer is decreased by any increase in solid volume fraction. Therefore, the local Nusselt number is enhanced by any increasing in solid volume fraction. On the other hand, for a stationary cylinder and for all Re, the variation of Nusselt found to be symmetrical at $\phi = 90°$. The value of the local Nu number is maximum on the front ($\phi = 0°$) and minimum on the rear ($\phi = 180°$) side of the cylinder. Also, at Re = 40, a kink is observed in the values of local Nusselt number. It can be explained on the basis that higher Reynolds number results in larger recirculation region. Also, the symmetrical variation of Nusselt in the figures for $\alpha = 0$ is lost under the effect of rotation. On increasing the value of the rotation rate, the local Nu number curve becomes smooth and the kink disappears. Finally, the rotation causes overall reduction in heat transfer across the cylinder, thus lowering the local Nusselt number at higher rotations.

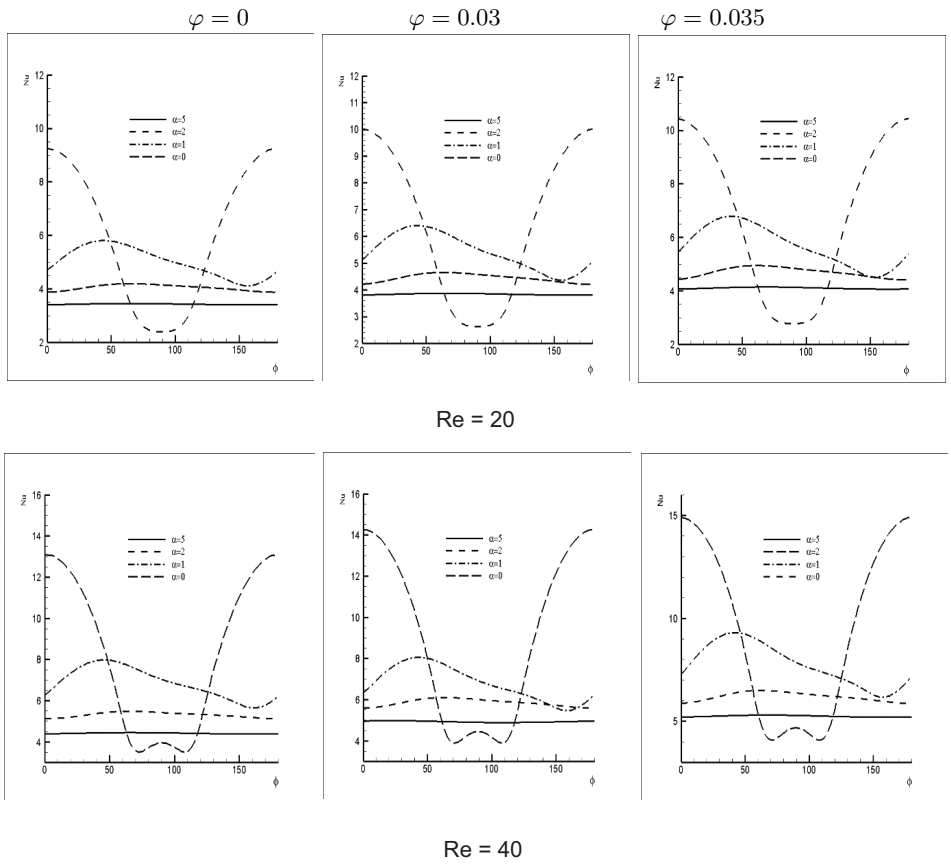

Figure 4: Local Nusselt number variation at various solid volume fractions (φ) for varying values of Reynolds number (Re) and rotation rate (α).

4.5 Averaged Nusselt number

The average Nusselt number variation is presented in Fig. 5 for the solid volume fraction varying from 0 to 0.05 in the steady regime. This figure indicates that the averaged Nusselt number increases linearly with increasing solid volume fraction of nanoparticles at different Reynolds numbers. This can be explained as when Reynolds number increases the inertia of flow increases thus increasing the heat transfer. The effect of Reynolds number also increases with increase in volume fraction number; the Reynolds and

Prandtl number of nanofluids can be expressed as:

$$\mathrm{Re}_{nf} = \frac{\rho_{nf}}{\rho_f}\frac{\mu_f}{\mu_{nf}}\mathrm{Re}\,, \quad \mathrm{Pr}_{nf} = \frac{\mu_{nf}}{\mu_f}\frac{C_{P,nf}}{C_{P,f}}\frac{k_f}{k_{nf}}\mathrm{Pr}\,. \tag{14}$$

Further, on increasing the value of the rotation rate for a fixed Reynolds number, the value of the average Nusselt number decreases for all values of solid volume fraction studied here. The decrease in the Nusselt number with increasing rotational velocity can be explained on the basis that the fluid entrapped inside the enveloping vortex acts as a buffer zone for heat transfer between the cylinder and free stream and restrict the heat transfer to conduction only, Fig. 6.

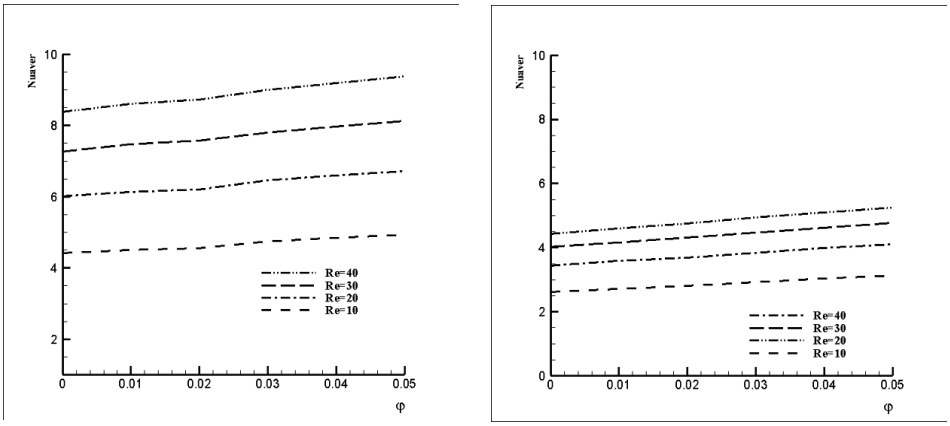

Figure 5: Variation of average Nusselt number at various solid volume fractions (φ) for varying values of Reynolds number (Re) and rotation rate (α).

Figure 7 illustrations the normalized Nusselt number obtained as the ratio of the average Nusselt number of the rotating cylinder ($\overline{\mathrm{Nu}}$) to that of a stationary cylinder (Nu_0) for base fluid and nanofluid ($\varphi = 0.05$) at various rotation rates, to understand the suppression of heat transfer. For φ of 0.05, It can be seen from this figure that the suppression increases with increasing Re and increasing α, with a minimum value of 15.29% for Re = 5 and a maximum value of 44.03% for Re = 40 at $\alpha = 5$. Thus, cylinder rotation can be used not only for controlling flow, but also as an efficient heat transfer suppression technique. Moreover, for the case of $\varphi = 0$, there is a remarkable increase in heat transfer suppression. Maximum heat suppression is 47.35% at Re of 40 and rotation rate α of 5. Decrease in Prandtl number significantly reduces the heat transfer suppression: the

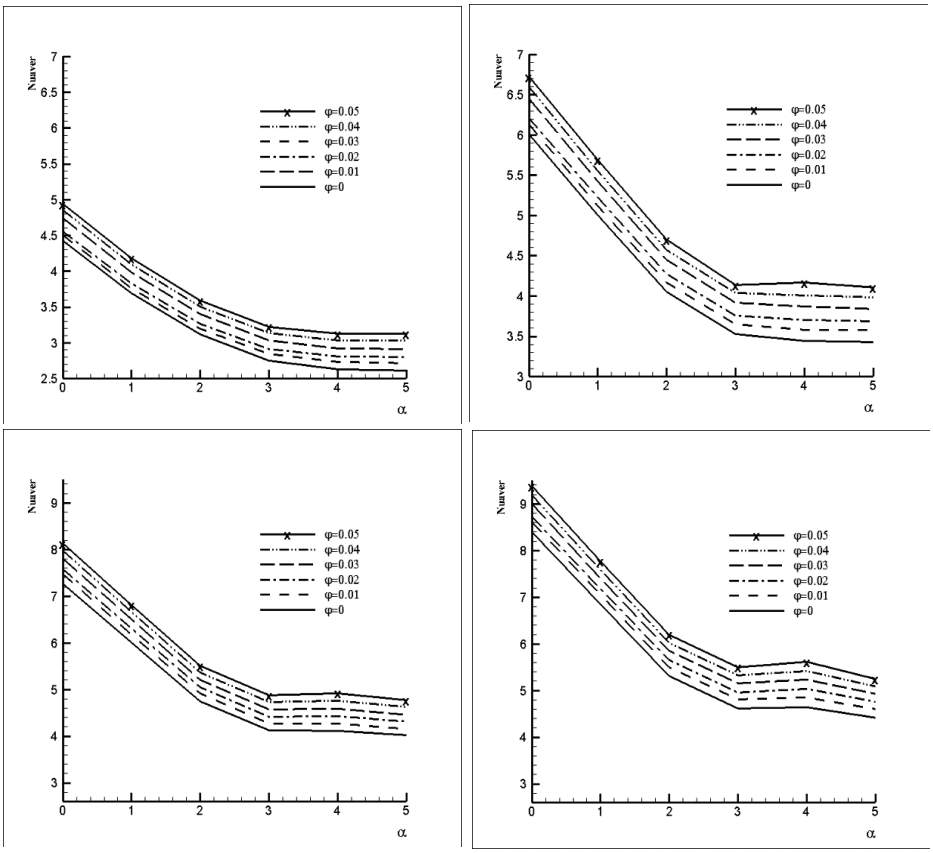

Figure 6: Variation of average Nusselt number on the wall of cylinder at different volume fractions (φ) for different Reynolds (Re) numbers and rotation raet (α).

change in the value of the Prandtl number for the case $\varphi = 0$ is in the range from 7.066 to 4.763 for the case $\varphi = 0.05$. Hence, the suppression of heat transfer is reduced due to adding nanoparticles into base fluid as shown in Fig. 8.

5 Conclusion

The present study focuses on the unconfined laminar flow of nanofluid and heat transfer characteristics around a rotating circular cylinder dissipating uniform heat flux in the steady regime. The illustrative streamline patterns and isotherm patterns are presented and examined for the above range of

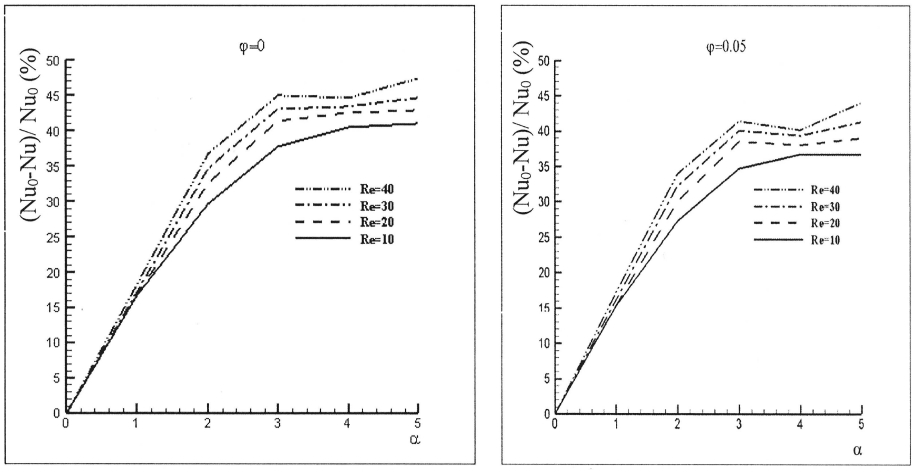

Figure 7: Percentage heat transfer suppression with increasing volume fractions (φ) for different Reynolds numbers (Re). Nu_0 is the Nusselt number of the stationary cylinder.

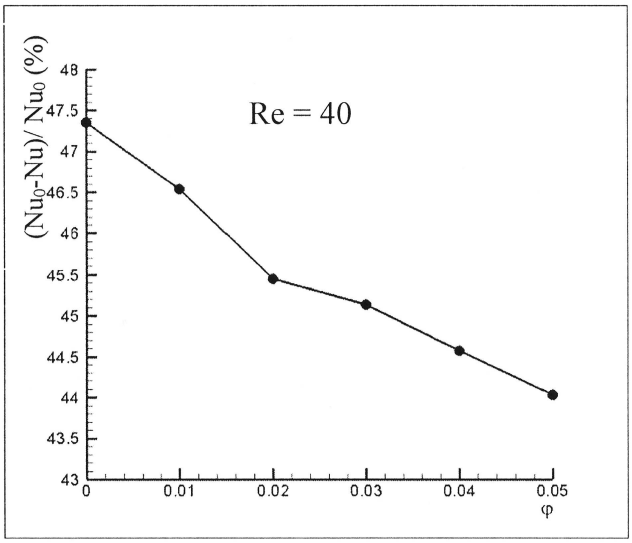

Figure 8: Percentage heat transfer suppression with increasing φ for Re = 40 and $\alpha = 5$.

conditions. It was showed that at a given Reynolds number, local and average Nusselt numbers were enhanced by adding nanoparticles to base fluid. Also, on increasing the value of the rotation rate for a fixed Reynolds number, the value of the average Nusselt number decreases for all values of solid volume fraction studied. Moreover, the heat transfer suppression of heat transfer is reduced due to adding solid nanoparticles into the base fluid.

Received 13 November 2017

References

[1] Paramane S.B., Sharma A.: *Numerical investigation of heat and fluid flow across a rotating circular cylinder maintained at constant temperature in 2D laminar flow regime*. Int. J. Heat Mass Tran. **52**(2009), 13–14, 3205–3216.

[2] Bouakkaz R. et al.: *Numerical investigation of incompressible fluid flow and heat transfer around a rotating circular cylinder*. Thermophys. Aeromech. **21**(2014), 1, 87–97.

[3] Sharma V., Dhiman A.K.: *Heat transfer from a rotating circular cylinder in the steady regime: Effects of Prandtl number*. Thermal Sci. **16**(2012), 1, 79–91.

[4] Sufyan M., Manzoor S., Sheikh N.A.: *Free stream flow and forced convection heat transfer across rotating circular cylinder in steady regime: effects of rotation, Prandtl number and thermal boundary condition*. J. Mech. Sci. Technol. **29**(2015), 4, 1781–1797.

[5] Paramane S.B., Sharma A.: *Heat and fluid flow across a rotating cylinder dissipating uniform heat flux in 2D laminar flow regime*. Int. J. Heat Mass Tran. **53**(2010), 21-22, 4672–4683.

[6] Bouakkaz R. et al.: *Unconfined laminar nanofluid flow and heat transfer around a rotating circular cylinder in the steady regime*. Arch. Thermodyn. **38**(2017), 2, 3–20.

[7] Khelili Y., Allali A., Bouakkaz R.: *Convective heat transfer characteristics of low Reynolds number nanofluid flow around a circular cylinder*. Metall. Mater. Eng. **23**(2017), 1, 83–97.

[8] Rup K., Nering K.: *Unsteady natural convection in micropolar nanofluids*. Arch. Thermodyn. **35**(2014), 3, 155–170.

[9] Valipour M.S., Ghadi A.Z.: *Numerical investigation of fluid flow and heat transfer around a solid circular cylinder utilizing nanofluid*. Int. Commun. Heat Mass **38**(2011), 1296–1304.

[10] El-Bashbeshy E.S.M.A, Emam T.G., Abdel-Wahed M.S.: *The effect of thermal radiation, heat generation and suction/injection on the mechanical proproperties of unsteady continuous moving cylinder in a ananofluid*. Thermal Science **19**(2015), 5, 1591–1601.

[11] Vegad M, Satadia S., Pradip P., Chirag P., Bhargav P.: *Heat transfer characteristics of low Reynolds number flow of nanofluid around a heated circular cylinder.* Procedia Technology **14**(2014), 348–356 (see also Proc. 2nd Int. Conf. on Innovations in Automation and Mechatronics Engineering, ICIAME 2014).

[12] Farooji V.E., Bajestan E.E., Niazmand H., Wongwises S.: *Unconfined laminar nanofluid flow and heat transfer around a square cylinder.* Int. J. Heat Mass Tran. **55**(2012), 1475–1485.

[13] Valipour M.S., Masoodi R., Rashidi S., Bovand M., Mirhosseini M.: *A numerical study on convection around a square cylinder using* AL_2O_3*-*H_2O *nanofluid.* Thermal Science **18**(2014), 4, 1305–1314.